journal of the mechanical behavior of biomedical materials 125 (2022) 104951

Contents lists available at ScienceDirect

Journal of the Mechanical Behavior of Biomedical Materials

journal homepage: www.elsevier.com/locate/jmbbm

Research Paper

Saline-polyethylene glycol blends preserve *in vitro* annulus fibrosus hydration and mechanics: An experimental and finite-element analysis

Benjamin Werbner [a], Minhao Zhou [a], Nicole McMindes [a], Allan Lee [b], Matthew Lee [a], Grace D. O'Connell [a,c,*]

[a] Department of Mechanical Engineering, University of California, Berkeley, USA
[b] Department of Bioengineering, University of California, Berkeley, USA
[c] Department of Orthopaedic Surgery, University of California, San Francisco, USA

ARTICLE INFO

Keywords:
Polyethylene glycol
Annulus fibrosus
Tissue hydration
Failure mechanics
Transient swelling
Multi-phasic finite-element modeling

ABSTRACT

Precise control of tissue water content is essential for ensuring accurate, repeatable, and physiologically relevant measurements of tissue mechanics and biochemical composition. While previous studies have found that saline and polyethylene glycol (PEG) blends were effective at controlling tendon and ligament hydration levels, this work has yet to be extended to the annulus fibrosus (AF). Thus, the first objective of this study was to determine and validate an optimal buffer solution for targeting and maintaining hydration levels of tissue-level AF specimens *in vitro*. This was accomplished by measuring the transient swelling behavior of bovine AF specimens in phosphate-buffered saline (PBS) and PEG buffers across a wide range of concentrations. Sub-failure, failure, and post-failure mechanics were measured to determine the relationship between changes in tissue hydration and tensile mechanical response. The effect of each buffer solution on tissue composition was also assessed. The second objective of this study was to assess the feasibility and effectiveness of using multi-phasic finite element models to investigate tissue swelling and mechanical responses in different external buffer solutions.

A solution containing 6.25%w/v PBS and 6.25%w/v PEG effectively maintained tissue-level AF specimen hydration at fresh-frozen levels after 18 h in solution. Modulus, failure stress, failure strain, and post-failure toughness of specimens soaked in this solution for 18 h closely matched those of fresh-frozen specimens. In contrast, specimens soaked in 0.9%w/v PBS swelled over 100% after 18 h and exhibited significantly diminished sub-failure and failure properties compared to fresh-frozen controls. The increased cross-sectional area with swelling contributed to but was not sufficient to explain the diminished mechanics of PBS-soaked specimens, suggesting additional sub-tissue scale mechanisms. Computational simulations of these specimens generally agreed with experimental results, highlighting the feasibility and importance of including a fluid-phase description when models aim to provide accurate predictions of biological tissue responses. As numerous previous studies suggest that tissue hydration plays a central role in maintaining proper mechanical and biological function, robust methods for controlling hydration levels are essential as the field advances in probing the relationship between tissue hydration, aging, injury, and disease.

1. Introduction

Water content is known to have a significant effect on tissue mechanics across length scales [Costi et al., 2002; Screen et al., 2006; Han et al., 2012; Bezci et al., 2015; Żak and Pezowicz, 2016; Werbner et al., 2019; Bloom et al., 2021]. Thus, buffer solutions have been used to maintain hydration levels during mechanical testing, achieve target water content values, and as treatment carriers for *in vitro* disease models [Skaggs et al., 1994; Acaroglu et al., 1995; Ebara et al., 1996; Screen et al., 2005; Lujan et al., 2009; Han et al., 2012; Isaacs et al., 2014; Bezci et al., 2015; Żak and Pezowicz, 2016; Werbner et al., 2019; Werbner et al., 2021 (*in review*)]. Additionally, buffer solutions may be used for short-term tissue storage during sample preparation and to correct minor dehydration occurring during dissection, sample

; AF, Annulus fibrosus; PEG, Polyethylene glycol; PBS, Phosphate-buffered saline; SPEG, Saline-polyethylene glycol blend; w/v, Weight/volume; FW, Fresh weight; DW, Dry weight; WC, Water content; EXP, Experimental; COM, Computational; CSA, Cross-sectional area.

* Corresponding author. 5122 Etcheverry Hall, #1740, Berkeley, CA, 94720-1740, USA.
E-mail address: g.oconnell@berkeley.edu (G.D. O'Connell).

https://doi.org/10.1016/j.jmbbm.2021.104951
Received 19 June 2021; Received in revised form 23 October 2021; Accepted 27 October 2021
Available online 2 November 2021

preparation, or imaging [Galante, 1967; Skaggs et al., 1994; Pflaster et al., 1997; Costi et al., 2002; Pezowicz et al., 2005; Żak and Pezowicz, 2016]. Precise control of tissue hydration levels is essential for ensuring accurate, repeatable, and physiologically relevant measurements of tissue mechanics and biochemical composition [Costi et al., 2021].

This is particularly important for joint-, tissue-, and sub-tissue level specimens that have been removed from larger, more constrained structures, as progressive dissection alters residual stresses and removes fluid-mediating barriers such as the cartilaginous endplate and longitudinal ligament. Thus, while 'physiological saline' (0.15M or 0.9%w/v phosphate-buffered saline, 'PBS') maintains intervertebral disc hydration *in vivo*, removal of the vertebral bodies and cartilage endplates dramatically alters tissue boundary conditions, leading to excessive swelling in both the annulus fibrosus (AF) and the nucleus pulposus (Fig. 1) [Urban and Maroudas, 1981; Skaggs et al., 1994; Acaroglu et al., 1995; Ebara et al., 1996; Pflaster et al., 1997; Han et al., 2012; Huyghe and Jongeneelen, 2012; Bezci et al., 2015; Bezci et al., 2020]. Furthermore, when tissue-level specimens are removed from the whole disc, additional swelling occurs, with outer AF specimens approximately doubling in size when allowed to free-swell in 0.9%w/v PBS [Han et al., 2012; Żak and Pezowicz, 2016; Werbner et al., 2019; Bezci et al., 2020]. This highlights the importance of developing solutions that maintain physiological hydration levels based on specific *in vitro* boundary conditions for a given experiment [Urban and Maroudas, 1981; Costi et al., 2002; Lujan et al., 2009; Huyghe and Jongeneelen, 2012].

To this end, previous studies have used hyperosmotic saline and sucrose solutions in an attempt to maintain physiological tissue hydration levels during long-duration mechanical testing experiments [Han et al., 2012; Bezci et al., 2015; Paul Buckley et al., 2016; Safa et al., 2017]. These studies and others showed that hyperosmotic saline solutions cause significant solute diffusion into the tissue, altering the biochemical environment, potentially affecting measured mechanics, and artificially inflating tissue dry weights, which confounds calculation of normalized biochemical components [Davey and Skegg, 1971; Safa et al., 2017; Werbner et al., 2019, Bezci et al., 2020]. Previous studies found that large molecular weight hydrophilic polymers, such as polyethylene glycol (PEG), were effective at controlling tissue hydration levels without significant solute deposition, likely because the large molecular weight prohibits the molecule from diffusing into the tissue [Davey and Skegg, 1971; Katz and Li, 1973; Robinson, 1978; Sverdlik and Lanir, 2002; Lujan et al., 2009; Huyghe and Jongeneelen, 2012; Safa et al., 2017; Bloom et al., 2021]. In particular, solutions containing a mixture of saline and PEG have been shown to robustly control tendon and ligament hydration levels with minimal solute deposition [Lujan et al., 2009; Safa et al., 2017; Bloom et al., 2021].

This work has yet to be extended to annulus fibrosus, which experiences even greater alterations in boundary conditions and swelling capacity than tendon when tested at the tissue level. Additionally, previous studies have not investigated the effects of such buffer solutions on tissue constituent composition after extended soak times, such as those required when using solutions as treatment carriers for disease-models (~18 h). Thus, the first objective of this study was to determine and validate an optimal buffer solution for targeting and maintaining hydration levels in tissue-level AF specimens. This was accomplished by measuring transient swelling behavior of bovine AF specimens in saline and PEG buffers across a wide range of concentrations. Sub-failure, failure, and post-failure uniaxial tensile mechanics were measured to determine the relationship between buffer solution induced changes in tissue hydration and tensile mechanical response. The effect of each buffer solution on tissue biochemical constituent composition was also assessed. Furthermore, despite theoretical and technological advances allowing computational models to describe tissue hydration and swelling, computational studies of the AF have not yet examined the effect of different external bath solutions on active tissue swelling and mechanical behavior, which is important to accurately match experimental testing conditions [Mow et al., 1980; Ateshian et al., 1994; Ateshian et al., 2004; Ehlers et al., 2009; Yang and O'Connell, 2018; Safa et al., 2020; Zhou et al., 2019, 2021]. Thus, the second objective of this study was to examine tissue swelling and mechanical response in candidate buffer solutions through computational simulation (multi-phasic finite element modeling). Fresh-frozen bovine AF tissue was used as the control for swelling, mechanical, biochemical, and computational analyses.

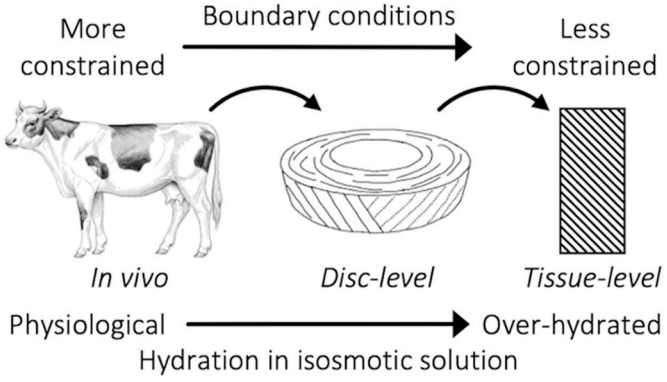

Fig. 1. As anatomically constraining boundary conditions are removed, tissue hydration increases from physiological to over-hydrated levels in isosmotic solutions.

2. Methods

2.1. Experimental testing

2.1.1. Transient and equilibrium swelling

Three fresh coccygeal spine sections from skeletally mature bovines (age ~18–24 months) were acquired from a local abattoir. Musculature was removed and discs were dissected from levels C2–C5 with a scalpel. Eight to ten middle-outer AF specimens were removed from each disc using a 4 mm biopsy punch and immediately massed to determine fresh tissue weight ('FW'); care was taken to produce specimens of nearly equal mass (198 ± 19.7 mg). Specimens were randomized and soaked at room temperature in 5 ml of buffer solution (n = 4 samples per solution concentration). Candidate buffer solutions were created by mixing a range of concentrations of PBS and PEG (Table 1). In particular, three solution compositions were investigated at each of the following concentration levels: 0.9, 5, 10, 15, and 20%w/v PBS ('PBS1'-'PBS20', respectively); 5, 10, 15, and 20%w/v PEG ('PEG5'-'PEG20', respectively), and one-to-one mixtures of 5, 10, 15, and 20%w/v PBS and 5, 10, 15, and 20%w/v PEG ('SPEG5'-'SPEG20', respectively). For example, SPEG10 was a mixture of equal parts 10%w/v PBS with 10%

Table 1
Weight/volume (w/v) and molar concentrations of buffer solutions: phosphate-buffered saline (PBS), polyethylene glycol (PEG), and saline-PEG blend (SPEG).

Solution	PBS Concentration		PEG Concentration	
Name	%w/v	mol/L	%w/v	mmol/L
PBS1	0.90	0.15	0.00	0.00
PBS5	5.00	0.86	0.00	0.00
PBS10	10.0	1.71	0.00	0.00
PBS15	15.0	2.57	0.00	0.00
PBS20	20.0	3.42	0.00	0.00
PEG5	0.00	0.00	5.00	2.50
PEG10	0.00	0.00	10.0	5.00
PEG15	0.00	0.00	15.0	7.50
PEG20	0.00	0.00	20.0	10.0
SPEG5	2.50	0.43	2.50	1.25
SPEG10	5.00	0.86	5.00	2.50
SPEG15	7.50	1.28	7.50	3.75
SPEG20	10.0	1.71	10.0	5.00

w/v PEG, resulting in a final concentration of 5%w/v PBS and 5%w/v PEG. All solutions were pH-balanced to 7.4. Solution compositions are detailed in Table 1.

To provide insight into the transient swelling behavior, specimens were briefly removed from their solutions, blotted dry to remove surface liquid, and weighed periodically during 18 h of free swelling ($TW_{x\ min}$ = transient weight at minute x). Swelling ratio was defined as the percent mass increase divided by the initial fresh weight (*e.g.*, swelling ratio at 120min = (TW_{120min}-FW)/FW × 100). After 18 h of free swelling, specimens were massed and lyophilized to determine tissue dry weight (DW), which was used to calculate water content (WC) during the fresh, transient, and soaked states (*e.g.*, WC_{120min} = (TW_{120min}-DW)/TW_{120min}).

2.1.2. Uniaxial tensile testing

Mechanical testing was performed for the best-performing candidate buffer solution (alongside fresh-frozen and PBS controls) to investigate whether the optimal swelling-limiting solution also maintained tensile mechanics. Thus, three additional fresh coccygeal spine sections were acquired from the same abattoir and discs were dissected from levels C2–C5. Rectangular specimens 2 mm thick and 5 mm wide were prepared from the middle-outer region of the anterior and posterior AF using a freezing stage microtome and oriented with the length along the circumferential direction and the width along the axial direction. Preliminary work ensured no differences in mechanics between anterior and posterior bovine AF (n = 6/group, $p > 0.3$; not shown). Specimen cross-sectional area (CSA) at the midlength was reduced to 1 mm thickness and 1.25 mm width using a series of custom cutting jigs [Werbner et al., 2021 (*in review*)]. That is, the initial cross-sectional area ('pre-CSA') was assumed to be 1.25 mm^2 for all mechanical test specimens. A similar notch geometry was previously developed and validated by our lab using a combined experimental and computational approach to ensure tissue failure properties were robustly and consistently measured [Werbner et al., 2017].

Samples in the SPEG group were soaked in a solution containing 6.25%w/v PBS and 6.25%w/v PEG pH-balanced to 7.4 (n = 6, 'SPEG') and specimens in the PBS group were soaked in 0.9%w/v PBS pH-balanced to 7.4 (n = 6, 'PBS'); all samples were soaked for 18 h at 25 °C prior to testing. Fresh-frozen samples were thawed at room temperature in damp gauze for 15 min immediately prior to testing (n = 6, 'Fresh'). Specimens were gripped for mechanical testing using custom-made, serrated screw-clamp grips. A monotonic 0.1 N preload was applied to remove slack from the tissue. Cyclic preconditioning was not applied to avoid altering pre-testing tissue water content, which could affect treatment groups differently [Schmidt et al., 2016]. High-resolution scale bar photographs were taken to measure sample-specific post-swelling cross-sectional area ('post-CSA') and gauge length (average gauge-length 10.1 ± 0.3 mm; ANOVA $p > 0.5$ between groups).

Uniaxial tension was applied monotonically along the circumferential direction at 6 mm/min (~1%/sec) until the specimen separated into two pieces with no load-bearing components between them (end-of-test load threshold = 0.2N). Engineering strain was calculated as the measured change in test-machine crosshead displacement divided by the initial gauge length. Engineering stress was calculated as the measured force divided by the initial cross-sectional area at the midlength. The linear-region modulus was calculated using a custom, sequential linear-regression optimization to the stress-strain response to ensure exclusion of the toe- and yield-regions. Briefly, the algorithm sequentially narrowed a window in which to fit the stress-strain response with a linear regression until the goodness of fit ceased to improve beyond a calibrated threshold. Failure stress was defined as the maximum stress and failure strain as the corresponding strain. Strain energy density was determined through numerical integration of the stress-strain response. The 'failure energy ratio' (FER) was defined as the strain energy density up to the point of failure divided by the total strain energy density (*i.e.*, until the end-of-test load threshold was achieved). Immediately after testing, two small tissue samples were removed from near the notch site, massed, and lyophilized to determine water content, as described above.

2.1.3. Biochemical analysis

All lyophilized samples were digested in 1 ml of 2 mg/mL proteinase K. Glycosaminoglycan (GAG) content was determined using the 1,9-dimethylmethylene blue assay [Farndale et al., 1982]. An aliquot of each digest was hydrolyzed in 6N HCl at 120 °C for 24 h, after which the HCl solution was allowed to evaporate completely under low heat (~40 °C). Lysates were resuspended and assayed for hydroxyproline using the chloramine-T spectrophotometric method [Stegemann and Stalder, 1967]. Collagen content was calculated assuming a 1:7.5 hydroxyproline-to-collagen mass ratio [Hollander et al., 1994]. Lysates were also assayed for advanced glycation end-product content (AGEs) as measured by total fluorescence using a quinine sulfate standard at excitation/emission wavelengths of 370 nm/440 nm.

2.2. Computational modeling

2.2.1. Transient and equilibrium swelling

Finite element models were created to represent the AF explants prepared for experimental transient swelling (Supplemental Fig. 1). AF explants for transient swelling were modeled at a one-to-one scale to the average experimental AF explant dimensions and all models contained 1000 hexagonal elements. A triphasic mixture framework was applied to describe tissue hydration [Lai et al., 1991; Ateshian et al., 2004]. A Holmes-Mow description was employed to describe strain-dependent tissue permeability, k (Equation (1)). In Equation (1), J was the determinant of the deformation gradient tensor ($\boldsymbol{F}$), k_0 represented hydraulic permeability in the reference condition (k_0 = 0.0064mm4/N·s), φ_0 represented the AF solid volume fraction (φ_0 = 0.2), α represented the power-law exponent (α = 2), and M represented the exponential strain-dependence coefficient (M = 4.8) [Mow et al., 1984; Iatridis et al., 1998; Gu et al., 1999; Beckstein et al., 2008; Cortes et al., 2014; O'Connell et al., 2015]. Model fixed charge density represented tissue GAG content and was set to −450 mmol/L based on data in the literature [Urban and Maroudas, 1979; Antoniou et al., 1996; Bezci et al., 2019].

$$k(J) = k_0 \left(\frac{J-\varphi_0}{1-\varphi_0}\right)^{\alpha} e^{\frac{1}{2}M\left(J^2-1\right)} \quad [1]$$

Based on the presumably minimal continuous fiber bundles present in the small, cubic AF explants used for experimental transient swelling, AF explant models were described as compressible hyperelastic materials using the Neo-Hookean description [Guo et al., 2012] (Equation (2)). In Equation (2), I_1 and I_2 were the first and second invariants of the right Cauchy-Green deformation tensor $\boldsymbol{C}$ ($\boldsymbol{C} = \boldsymbol{F}^T\boldsymbol{F}$), and E_{matrix} and ν_{matrix} represented Young's modulus and Poisson's ratio, respectively. The modulus value (E_{matrix} = 1.5 MPa) was obtained from bovine single lamellar AF measurements *in vitro* [Monaco et al., 2016]. Specimens in Monaco et al. were misted with PBS during *in vitro* testing, which likely limited the amount of tissue swelling. The matrix Poisson's ratio (ν_{matrix} = 0.3) was obtained from human AF measurements *in vitro*, assuming comparable tissue properties [Cao et al., 2009; Bezci et al., 2019].

$$W_{matrix}(I_1, I_2, J) = \frac{E_{matrix}}{4(1+\nu_{matrix})}(I_1 - 3) - \frac{E_{matrix}}{2(1+\nu_{matrix})} lnJ + \frac{E_{matrix}\,\nu_{matrix}}{(1+\nu_{matrix})(1-2\nu_{matrix})}(lnJ)^2 \quad [2]$$

Three different external bath compositions were simulated to replicate the three solution compositions used in the experiments (PBS, PEG, and SPEG); thus, a total of 14 transient swelling simulations were performed (*i.e.*, PBS1-20, PEG5-20, SPEG5-20; solutions detailed in Table 1). For PBS solutions, it was assumed that 100% of the specimen pores could accommodate Na^+ and Cl^- ions [Maas et al., 2012; Bezci et al., 2015]. Osmotic coefficients for PBS solutions were determined directly from the respective solute concentrations at 25 °C [Partanen et al., 2017]. Previous studies reported that "PEG 4000 does not interact with nor penetrate collagen fibrils in any significant amount," [Katz and Li, 1973] and that "it is reasonable to assume that PEG 20000 penetrates [into the tissue] even less [than PEG 4000], because of its higher molecular weight" [Sverdlik and Lanir, 2002]. Thus, it was assumed that a minimal fraction of the specimen pores would accommodate PEG 20000. However, the FEBio solver requires a non-zero value for model convergence [Maas et al., 2012]. Based on preliminary parametric analysis to determine the minimum acceptable value ensuring the convergence of all models (analysis not shown), the pore fraction defined to accommodate PEG was set to 10%. As this value was not representative of a measured experimental parameter, but rather used purely numerically, it is considered unphysical in the context of this study. To the best of our knowledge, osmotic coefficients for multi-solute solutions containing PEG have not been experimentally measured or reported in the literature. Osmotic coefficients of PEG and SPEG specimens were calibrated to optimize agreement between model-predicted and experimental swelling responses in order to generate novel data for these coefficients and are thus presented as results below.

During transient swelling simulations, all degrees of freedom were constrained at a randomly selected surface of the AF explant model to ensure model stability. 18 h of swelling was simulated using transient swelling analyses. Tissue swelling ratio was calculated as the difference between pre- and post-swelling weight divided by the pre-swelling weight, assuming a tissue density of 1 g/cm^3.

2.2.2. Uniaxial tensile testing

Finite element models were developed to represent rectangular, uniaxial AF test specimens oriented along the circumferential-axial direction and were modeled at a one-to-one scale to the average initial experimental specimen dimensions (Supplemental Fig. 1). The lamellar thickness (0.4 mm) was determined based on values from single-lamellar studies [Holzapfel et al., 2005; Pham et al., 2018]. A notch was modeled at the midlength to replicate the experimental specimen geometry. All mechanical testing models contained ~92k hexagonal elements.

Fiber-reinforced strain energy continuum finite element models were used to describe the angle-ply AF structure [Spencer 1972]. The extrafibrillar matrix was modeled as described above (Equation (2)). Fibers were oriented at ±35° to the anatomical transverse plane to represent specimens from the middle-outer AF [Cassidy et al., 1989]. Fibers were modeled using a power-linear fiber strain energy density function, where β represented the power-law exponent in the toe-region, E_{lin} represented the fiber modulus in the linear-region, λ_0 represented the transition stretch between the toe- and linear-regions, and B was a function of β, E_{lin}, and λ_0 ($B = \frac{E_{lin}}{2}\left(\frac{(\lambda_0{}^2-1)}{2(\beta-1)} + \lambda_0{}^2\right)$; Equation (3)). Fiber parameters ($\beta = 6.0$, $E_{lin} = 400$ MPa, and $\lambda_0 = 1.15$) were determined based on our previously validated models [Werbner et al., 2017; Zhou et al., 2019; Zhou et al., 2021a, b], and experimental data of type I collagen in tension [Fratzl et al., 1998; Gentleman et al., 2003; Van Der Rijt et al., 2006; Shen et al., 2008].

$$\psi_n(\lambda_n) = \begin{cases} 0 & \lambda_n < 1 \\ \frac{E_{lin}}{4\beta(\beta-1)}\left(\lambda_0{}^2 - 1\right)^{2-\beta}(\lambda_n - 1)^{\beta} & 1 \le \lambda_n \le \lambda_0 \\ E_{lin}(\lambda_n - \lambda_0) + B\left(\lambda_n{}^2 - \lambda_0{}^2\right) + \frac{E_{lin}}{4\beta(\beta-1)}\left(\lambda_0{}^2 - 1\right)^{2-\beta}(\lambda_n - 1)^{\beta} & \lambda_n > \lambda_0 \end{cases} \quad [3]$$

The triphasic mixture framework applied in the transient swelling models was also applied to all mechanical testing specimens to account for tissue swelling. Three different hydration conditions were simulated to replicate the three experimental groups (Fresh, PBS, and SPEG); one model with average experimental specimen dimensions was simulated for each condition. No external bath was modeled for the Fresh specimen. The external bath for the PBS model contained 0.154 M NaCl (*i.e.*, 0.9%w/v PBS), and 100% of the tissue pores were assumed to accommodate these ions. The external bath for the SPEG model contained 1.069 M NaCl and 3.125 mM PEG (molecular weight: 20 kDa), which was equivalent to the SPEG solution used in the mechanical testing experiments. As above, the pore fraction accommodating PEG was set at 10%. To assess the effect of including a description for tissue hydration and osmotic response on predicted mechanical behavior, a single-phasic hyperelastic tissue model, which has been commonly used in finite element models of biological soft tissues, was also created. The model shared identical solid phase material parameters with the three triphasic models described above but did not describe the tissue fluid phase or the external bath solution.

PBS and SPEG models were loaded in a two-step process: First, free swelling was simulated in the respective external bath solution. Then, a uniaxial tensile ramp to 50% engineering strain was applied. Since no external bath was modeled for Fresh and hyperelastic models, only the second step was employed. All models were simulated using steady-state analyses and the model output was evaluated at equilibrium. Linear-region modulus was calculated as the slope of the linear-region of the engineering stress-strain response.

2.3. Statistical analysis

Values are reported as medians (first quartile: third quartile). Figure error bars indicate interquartile ranges. Bivariate linear

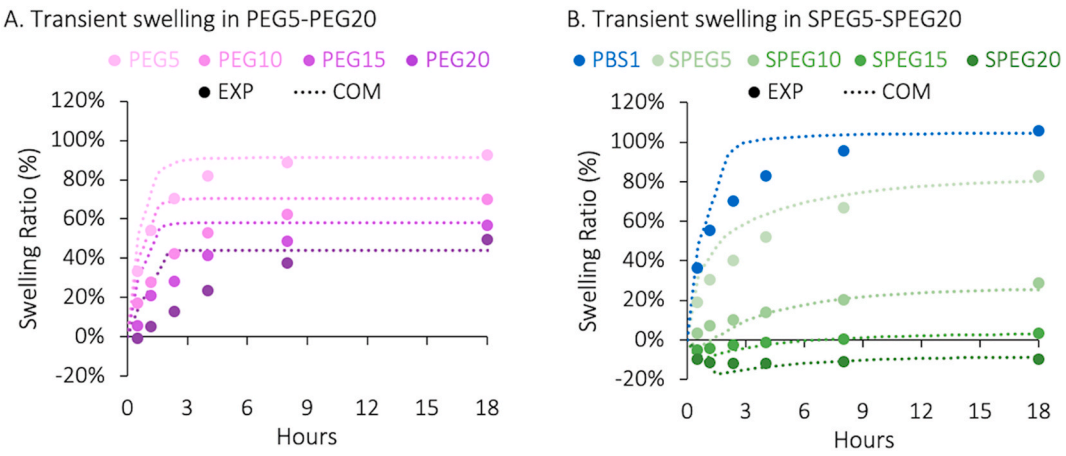

Fig. 2. Experimental (EXP) and computational (COM) transient swelling trends for specimens in (A) PEG and (B) SPEG buffer solutions. PBS1 is shown for comparison. Each point represents the median of 4 EXP samples and dotted lines represent COM results. Select values and variance are given in Table 2 and Supplemental Table 2. Logarithmic curve-fits to experimental results are given in Supplemental Table 1.

Table 2
Transient experimental swelling values in PBS, PEG, and SPEG for a range of concentrations. Values represent the median (interquartile range) of 4 samples.

Solution	30min	8hr	18hr
PBS1	36% (32:39%)	96% (91:99%)	106% (97:113%)
PBS5	27% (26:28%)	99% (94:105%)	110% (108:117%)
PBS10	19% (18:20%)	93% (89:98%)	110% (107:114%)
PBS15	20% (18:21%)	89% (84:95%)	103% (99:108%)
PBS20	8.7% (8.2:11%)	70% (68:76%)	92% (90:97%)
PEG5	33% (32:34%)	89% (83:93%)	92% (89:97%)
PEG10	17% (14:20%)	62% (57:66%)	70% (63:72%)
PEG15	5.6% (4.1:7.2%)	49% (43:55%)	57% (50:64%)
PEG20	−0.7% (−2.0:0.4%)	38% (33:42%)	50% (45:53%)
SPEG5	19% (17:21%)	67% (63:68%)	83% (78:85%)
SPEG10	3.4% (3.0:4.4%)	20% (18:22%)	29% (28:30%)
SPEG15	−5.1% (−5.5:4.3%)	0.4% (−0.8:3.0%)	3.4% (2.3:6.3%)
SPEG20	−9.7% (−11:9.5%)	−11% (−13:9.2%)	−9.6% (−12:8.1%)

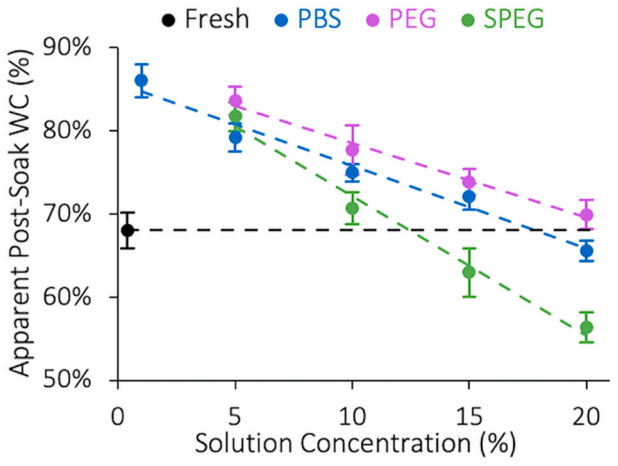

Fig. 3. Median EXP apparent tissue water content after 18 h in solution (n = 4 per data point). Some values, particularly in the PBS group, may appear lower than true values due to inferred solute deposition. Trendlines represent linear regression ($R^2 > 0.97$).

correlations were established between solution concentrations and hydration levels and considered valid for correlation coefficients $R^2 > 0.70$. One-way ANOVA analyses were performed on all mechanical and biochemical properties; significance for ANOVA was assumed at $p < 0.05$. Dunnett's method was applied for multiple pairwise comparisons

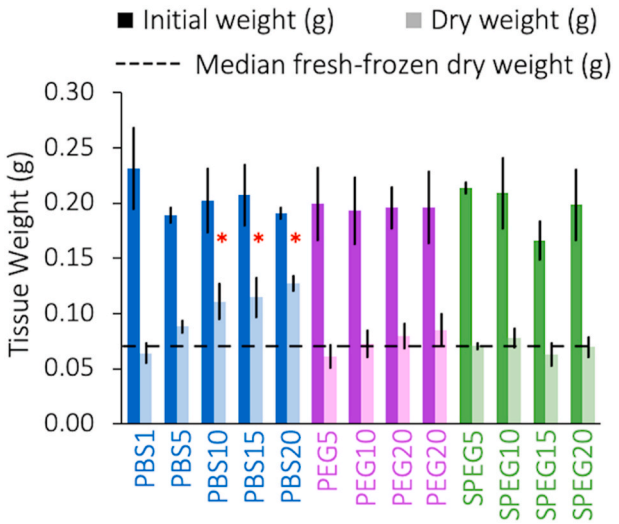

Fig. 4. Median and interquartile range of EXP initial and dry weights (n = 4 per group). For the PBS groups, dry weights increased with osmolarity despite similar initial weights, indirectly suggesting solute deposition in these groups. * indicates Dunnett's $p < 0.001$ vs fresh-frozen dry weights.

Table 3
Linear-region modulus (E) for EXP and COM specimens; failure stress (σ_f), failure strain (ε_f), failure energy ratio (FER), and percent change in gauge cross-sectional area (Δ-CSA) for EXP specimens. EXP values represent the median (interquartile range) of 6 samples.

Solution	EXP E (MPa)	COM E (MPa)	EXP σ_f (MPa)	EXP ε_f (%)	EXP FER (%)	EXP Δ-CSA (%)
Fresh	66 (54:71)	63	18 (16:20)	52 (49:56)	66 (61:75)	−2% (−9:6%)
PBS	13 (9:14)	25	3.8 (2.4:4.0)	53 (46:58)	48 (43:51)	82% (68:95%)
SPEG	74 (71:76)	79	20 (20:21)	49 (48:51)	64 (60:72)	−5% (−8:1%)

where significance was found, with the fresh-frozen group as the control (post-hoc significance assumed at $p < 0.05$).

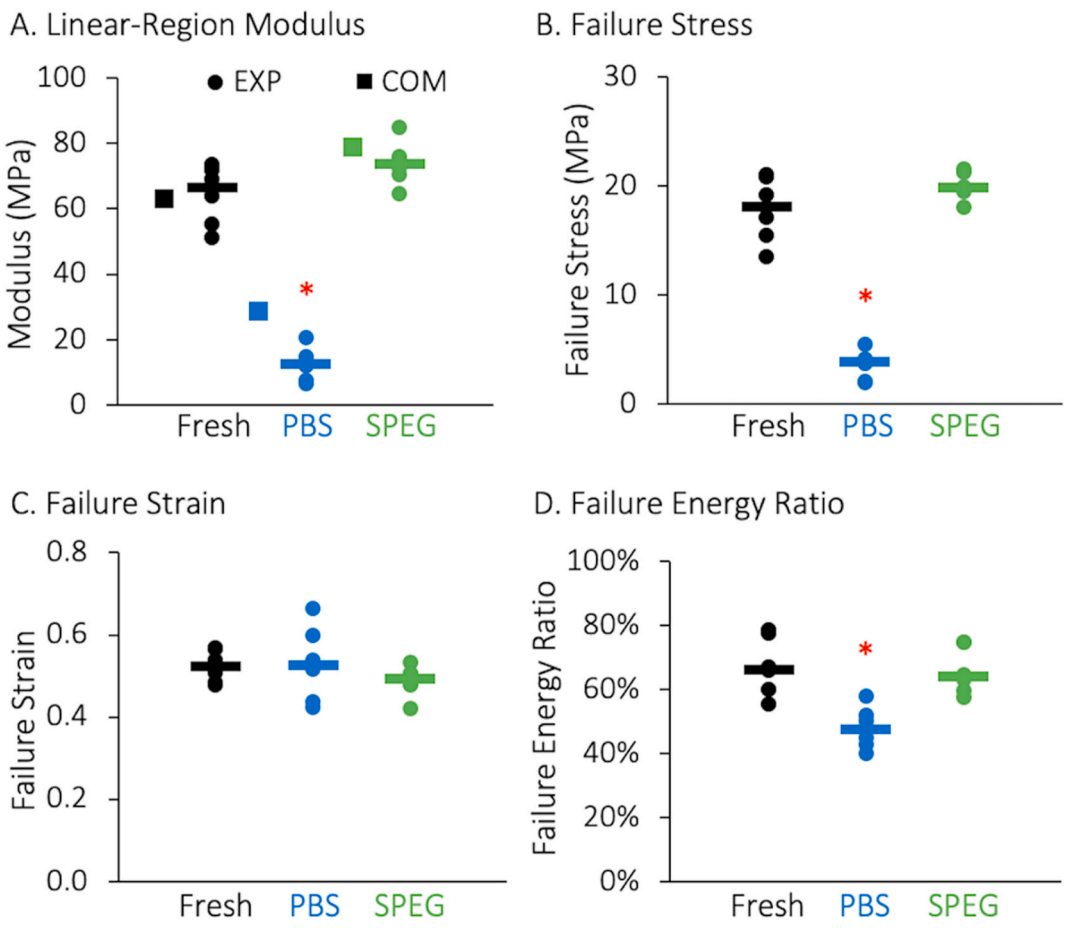

Fig. 5. (A) Linear-region modulus, (B) failure stress, (C) failure strain, and (D) failure energy ratio for each mechanical testing group. Bars represent EXP group medians. Squares represent COM modulus values. * indicates Dunnett's $p < 0.001$ vs fresh-frozen.

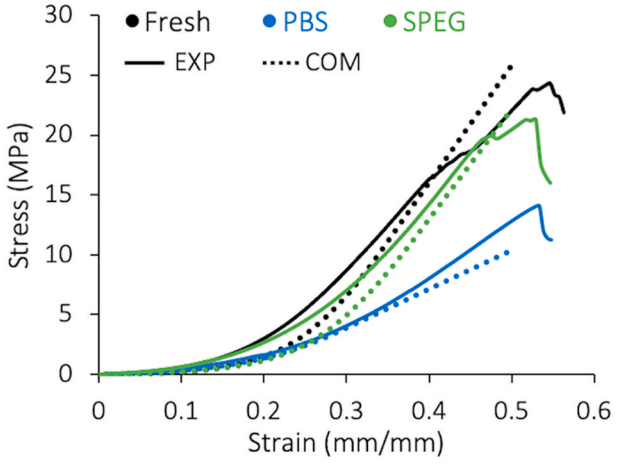

Fig. 6. Representative EXP and COM stress-strain curves. EXP curves have been truncated after failure for clarity; COM simulations were run to 50% engineering strain.

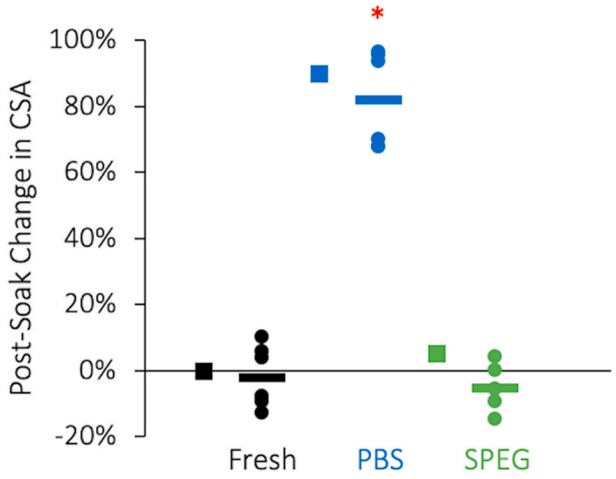

Fig. 7. Percent change in EXP (dots and bars) and COM (squares) mechanical test specimen gauge cross-sectional area (CSA) after 18 h in solution.

3. Results

3.1. Experimental testing

3.1.1. Transient and equilibrium swelling

A nonlinear transient swelling response was observed for all AF specimens soaked in PBS, PEG, and SPEG solutions (Fig. 2). Median and interquartile swelling data at select time points are reported in Table 2. Experimental transient swelling data for each solution was curve-fit with a logarithmic function ($R^2 > 0.93$ for all but SPEG20); curve-fit coefficients and goodness of fits for each solution are given in Supplemental Table 1.

Apparent equilibrium tissue water content after soaking in PBS, PEG, and SPEG is presented in Fig. 3. The relationship between solution concentration and measured post-soak water content was curve fit with

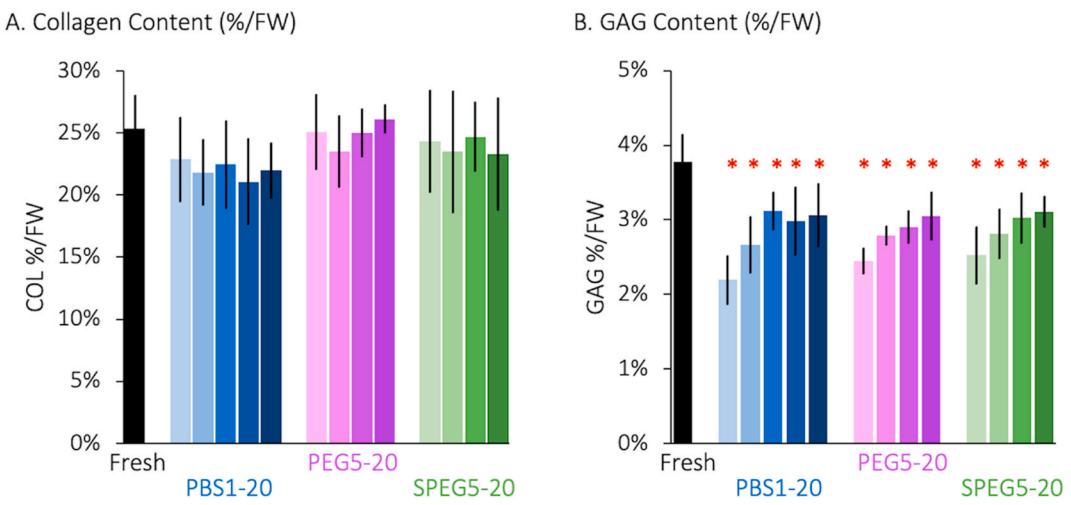

Fig. 8. (A) Collagen content and (B) GAG content normalized by tissue fresh weight. Each bar represents the median of 4 samples and error bars denote the interquartile range. * indicates Dunnett's p < 0.001 vs fresh-frozen.

a linear function ($R^2 > 0.97$ for all). Linear interpolation determined that the solution concentration required to achieve the median fresh-frozen tissue water content level was 15.7%w/v for PBS, 21.7%w/v for PEG, and 6.25%w/v PBS +6.25%w/v PEG for SPEG. Despite similar initial weights for all samples ($p > 0.2$), specimen dry weights increased significantly and progressively for PBS concentrations above 5%w/v (Dunnett's $p < 0.001$ versus fresh-frozen; Fig. 4). This increase in dry weights indirectly suggests solute deposition within the tissue, which may cause water content values to appear lower than true values for these groups [Safa et al., 2017]. Dry weights for PEG and SPEG specimens were not significantly different from controls for any solution concentration ($p > 0.4$; Fig. 4).

3.1.2. Uniaxial tensile testing

Mechanical testing results are summarized in Table 3 and Fig. 5 and representative stress-strain curves for experimental and computational samples are given in Fig. 6. A one-way ANOVA indicated significant differences in linear-region modulus, failure stress, and failure energy ratio ($p < 0.001$), but not failure strain ($p = 0.47$) between solution types. Specimens soaked in 0.9%w/v PBS exhibited an 81% decrease in modulus ($p < 0.0001$), a 79% decrease in failure stress ($p < 0.0001$), and a 27% decrease in failure energy ratio ($p = 0.001$) versus fresh-frozen controls (Fig. 5A, B, and D – red stars), concurrent with an 82% increase in gauge cross-sectional area (Fig. 7). In contrast, none of the mechanical properties of SPEG specimens were significantly different from fresh-frozen controls ($p > 0.10$; Figs. 5 and 6); gauge cross-sectional area was decreased by 5% after soaking (Fig. 7).

3.1.3. Biochemical analysis

Collagen content normalized by tissue fresh weight was not significantly different from fresh-frozen controls for any buffer solution ($p > 0.09$; Fig. 8A). However, when normalized by tissue dry weight, collagen content appeared to decrease by up to 58% for hyperosmotic PBS solutions versus fresh-frozen controls ($p < 0.001$), likely due to artificially elevated tissue dry weights caused by inferred solute deposition (Fig. 4). In contrast, GAG contents for specimens soaked in all buffer solutions were significantly lower than fresh-frozen controls, regardless of normalization method ($p < 0.05$ for GAG%/FW, $p < 0.02$ for GAG %/DW), indicating the likelihood of significant GAG leaching in all solutions (Fig. 8B – red stars). When normalized by tissue fresh weight, which would not be influenced by solute deposition, GAG leaching ranged from 18 to 42% versus fresh-frozen controls. AGE content normalized by tissue fresh weight was not significantly different from fresh-frozen controls for any buffer solution ($p > 0.18$), nor was AGE content normalized by collagen mass ($p > 0.40$).

3.2. Computational modeling

3.2.1. Transient and equilibrium swelling

Transient swelling responses generally agreed with experimental swelling responses for all solution compositions and concentrations (Fig. 2 – dashed lines). The osmotic coefficients for PBS1-20 specimens were 0.93, 0.93, 0.96, 1.0, and 1.05, respectively. The osmotic coefficients for PEG5-20 were all 0.5 and the osmotic coefficients for SPEG5-20 were 2.0, 1.5, 0.9, and 0.85, respectively.

3.2.2. Uniaxial tensile testing

For the PBS mechanical test specimen, the model-predicted equilibrium swelling ratio was 77%, with a 90% increase in model cross-sectional area. For the SPEG mechanical test specimen, the model-predicted equilibrium swelling ratio was 7%, with a 5% increase in model cross-sectional area. The linear-region modulus was 28.7 MPa for the PBS specimen, 78.8 MPa for the SPEG specimen, and 63.0 MPa for the Fresh specimen, directionally matching the experimental mechanical testing results (Figs. 5 and 6). Linear-region modulus of the single-phasic specimen was 39.5 MPa, which was 37% smaller than that of the triphasic Fresh model.

4. Discussion

This study investigated the effects of saline, PEG, and saline-PEG buffer solutions on AF transient and equilibrium swelling behavior and tensile mechanical properties using experimental and computational approaches. Buffer solution compositions and concentrations targeting a range of tissue-level AF hydration levels– including the maintenance of fresh-frozen hydration levels– were identified and tested *in vitro* to assess tissue swelling, mechanics, and biochemical composition, and *in silico* to assess tissue swelling and mechanics.

We found that a 6.25%w/v PBS and 6.25%w/v PEG solution (adjusted to pH 7.4) effectively maintained fresh-frozen AF tissue hydration levels, even after 18 h in solution (Table 2, Figs. 2–3). In addition to maintaining physiologic hydration levels, this solution also maintained tissue cross-sectional area, as well as sub-failure, failure, and post-failure tensile mechanics at fresh-frozen levels (Table 3, Figs. 5–7). In contrast, specimens soaked in 0.9%w/v PBS for 18 h experienced over 100% swelling (*i.e.*, absorbed more than their fresh weight in additional water), concurrent with an 80% increase in gauge cross-sectional area. Linear-region modulus and failure stress decreased nearly two-fold for

these samples versus fresh-frozen controls. Computational results generally agreed with the experimental measurements, matching the trends transient and equilibrium swelling responses across a range of buffer solution compositions and concentrations and indicating that tissue modulus values differed nearly two-fold between fresh-frozen and PBS-soaked specimens. The inclusion of a single-phasic hyperelastic model demonstrated that simply excluding the specimen fluid phase and external bath could decrease the apparent tissue modulus by ~40% versus fresh-frozen. Thus, these results demonstrate the feasibility and importance of including the tissue fluid phase and the surrounding chemical environment when models aim to provide accurate predictions of the mechanical response of hydrated biological tissues [Yang and O'Connell, 2018; Yang and O'Connell, 2019].

It appears that changes in water content likely influence tissue mechanics both by altering bulk specimen geometry due to swelling and by additional sub-tissue scale mechanisms not measured in the current study. At the tissue-level, the 80% increase in cross-sectional area for samples soaked in 0.9%w/v PBS would be expected to decrease the apparent modulus to ~37 MPa (from ~66 MPa for fresh tissue). However, we observed a significantly lower linear-region modulus for PBS-soaked specimens (~13 MPa), agreeing well with results reported by Żak and Pezowicz (2016) and adding to the emerging evidence that sub-tissue scale mechanisms likely contribute to diminished tissue stiffness with overhydration [Screen et al., 2006; Han et al., 2012; Żak and Pezowicz, 2016]. Such effects likely include: the leaching of GAGs, which has been shown to diminish AF single- and multi-lamellar tensile mechanics [Han et al., 2012; Isaacs et al., 2014; Werbner et al., 2019], increased distance between collagen fibrils [Screen et al., 2005; Screen et al., 2006; Han et al., 2012], and increased collagen fibril diameter, which has been associated with decreased tensile stiffness [Roeder et al., 2002; Buehler and Wong, 2007; Aladin et al., 2010]. Interestingly, the increase in model CSA was nearly sufficient to explain the observed changes in model-predicted modulus (*i.e.*, 33 MPa predicted by CSA-change vs 28 MPa measured *in silico*). This partially corroborates the hypothesis that sub-tissue level molecular interactions between collagen fibrils, matrix, and water molecules– which were not explicitly accounted for in the homogenized model used here– may help explain the larger reduction in modulus observed experimentally. Additionally, understanding the fundamental mechanisms driving altered failure mechanics is important as the field progresses towards a more comprehensive multi-scale understanding of multi-phasic tissue mechanics. However, it has proven difficult to determine the sub-tissue level mechanisms that drive the initiation of bulk tissue failure, as the current finite-element solver is not equipped to simulate tissue failure.

Significant developments in finite element modeling over the last two decades have allowed for investigations into the relationship between tissue fluid phase and mechanics. For example, poroelastic material descriptions have been used to investigate the stress-bearing role of interstitial water content and time-dependent rheological behavior [Natarajan et al., 2006; Wilson et al., 2007; Galbusera et al., 2011a, b; Barthelemy et al., 2016; Rijsbergen et al., 2018; Castro and Alves, 2021]. Despite these advances, few computational studies investigating tissue mechanics have employed material descriptions that adequately represent Donnan equilibrium effects, which play a pivotal role in active tissue swelling, mechanics, and metabolic behavior [Jacobs et al., 2014; Yang and O'Connell, 2018; Zhou et al., 2019; Zhou et al., 2021a, b]. Thus, it is noteworthy that the transient swelling simulations conducted in the current study agreed so well with the experiment results (Fig. 2). Despite this success, some substantial discrepancies were observed between computational simulations and experimental transient swelling trends during the first few hours. For example, transient rheological kinetics are expected to depend on specimen geometry (*e.g.*, surface area to volume ratio, residual stress profile, *etc.*) and local variations in composition (*e.g.*, heterogenous distribution of GAGs and collagen), which were not accounted for by the computational model. Additionally, the osmotic coefficient of a solution may change during the swelling period; however due to a lack of experimental data measuring transient osmotic coefficients, it was assumed to be constant in our simulations. Similarly, solute concentration in the simulation was assumed to be constant, providing a continuous environmental supply of solute and fluid, whereas in experiments, solute or fluid transfer to tissue is expected to alter the local external bath concentration and osmotic pressure, which in turn will alter the driving force for tissue swelling [Urban and Maroudas, 1979]. While the current study was not equipped to quantify these effects, we hope that this work will motivate and guide future studies to investigate these important issues influencing tissue transient swelling behavior.

None of the buffer solutions investigated in this study altered tissue collagen content when normalized by specimen fresh weight (Fig. 8). However, elevation of tissue dry weights in hyperosmotic saline solutions, presumably due to solute deposition, caused a significant decrease in apparent collagen content. For this reason, biochemical measurements from tissues exposed to hyperosmotic solutions should be normalized to specimen fresh weight [Bezci et al., 2019; Werbner et al., 2019]. A similar discrepancy between fresh and dry weight normalizations was observed for tissue AGE contents; it remains preferable to normalize AGE content to total collagen mass to avoid artifacts of solute deposition and account for inter-species differences in tissue collagen content [Showalter et al., 2012; Werbner et al., 2019 (*in review)*]. GAG contents were observed to decrease for all buffer solutions, regardless of normalization method, suggesting significant leaching of GAGs during extended soak times, agreeing well with previous observations [Urban and Maroudas, 1979; Maroudas et al., 1985; Perie et al., 2006; Han et al., 2012; Bezci et al., 2019; Bezci et al., 2020]. GAG content of specimens soaked in 0.9%w/v PBS suggest almost 50% loss in GAG content compared to fresh-frozen controls, while specimens soaked in SPEG20 lost less than 20% compared to fresh-frozen controls (Fig. 8). Thus, high-concentration saline-PEG blends provide the additional utility of limiting GAG leaching in addition to preserving fresh-frozen hydration levels and mechanical properties, consistent with previous literature reporting that 20 kDa PEG was used to help limit tissue GAG loss [Urban and Maroudas, 1979].

The main results of this study are consistent with recent tendon studies, which found that saline-PEG blends maintained hydration at fresh-frozen levels and limited the significant decrease in modulus observed after soaking in 0.9%w/v PBS [Safa et al., 2017; Bloom et al., 2021]. Additionally, Safa et al. (2017) showed that both NaCl and PEG have the same proportionate effect on lowering tendon water content at increasing concentrations, as indicated by the slopes in Table 3 and Fig. 4 of that study; while absolute water content values differ between tissue types (~55% in fresh tendon versus ~75% in fresh AF), this is directionally consistent with the results of this study (Fig. 3). Furthermore, the increased slope of the SPEG curve compared to NaCl and PEG in Safa et al. (2017) suggests that there is a substantial synergistic effect of combining these two solutes, consistent with the greater slope of the green line in Fig. 3. This important result is also consistent with older work by Davey and Skegg (1971) showing that media containing NaCl and PEG reduced kidney tissue water content *in vitro* by ~20–45% (depending on incubation time) compared to PEG- or NaCl-containing media alone. Interestingly, the model in this study resulted in a nonlinear decrease in osmotic coefficients as the PEG concentration increased in SPEG solutions, indicating that PEG likely affects NaCl osmotic activity. In addition to the experimental observations discussed above, these results also corroborate work by Schiller et al. (1988) suggesting that PEG might reduce the availability of water to interact with other osmotic solutes within the same solution. As the osmotic activity of solutions containing multiple solutes is difficult to characterize experimentally, multiphasic finite-element models may provide an effective tool to explore the osmotic effects of solutions containing multiple solutes.

The current study expands upon these results for the AF by presenting comprehensive transient swelling trends for a broad range of

buffer solution compositions and concentrations across an extended timescale (18 h). Despite these advances, this study had its limitations in the relatively small intra-group sample size for swelling experiments (n = 4 per solution concentration), the single specimen orientation used for mechanical testing (circumferential-axial), and single loading rate (~1%/sec), as previous studies have shown that AF mechanical response is orientation- and rate-dependent [Gregory and Callaghan, 2010; Isaacs et al., 2014; Werbner et al., 2017]. An additional limitation of the study was our choice to limit the study size by investigating only one-to-one mixtures of PBS and PEG. This choice arose from preliminary work which found that, even when paired with high concentrations of PEG, mixtures of 0.9%w/v NaCl were insufficient to limit tissue-level AF swelling (not shown). The discrepancy between this result and those observed previously in tendons and ligaments for 0.9%w/v NaCl +8% w/v PEG solutions [Sverdlik and Lanir, 2002; Lujan et al., 2009; Safa et al., 2017; Bloom et al., 2021] may be due to the substantially higher GAG content of AF samples (8–12%/DW in AF versus 1–5%/DW in tendon) [Demers et al., 2004; Thorpe and Screen, 2016], as well as potentially greater residual stresses in the AF due to *in situ* boundary conditions [Huyghe and Jongeneelen, 2012]. Additional work is needed to evaluate whether different ratios of PBS and PEG would produce similar (or possibly better) results in AF swelling.

This study determined and validated a saline-PEG buffer solution that maintained AF tissue-level hydration and mechanics *in vitro* at fresh-frozen tissue levels. The results from this study suggest that 0.9% w/v PBS should not be used to maintain tissue-level AF specimen hydration during preparation, treatment, or testing if physiological relevance is to be considered regarding hydration and mechanics. Instead, a solution generating sufficient osmotic pressure to maintain physiological hydration levels in tissue-level specimens should be used. While a 6.25%w/v PBS +6.25%w/v PEG solution proved effective for healthy bovine AF tissues commonly used in the field, inter-species differences and tissue health status are known to influence swelling and mechanical behavior; thus, future work should seek to determine optimal solution compositions to maintain hydration levels and mechanics in the specific tissues being studied. As the field develops a deeper understanding of the central role of tissue hydration in maintaining proper mechanical and biological function, it is essential for future studies investigating the relationship between tissue hydration, aging, injury, and disease to prepare, treat, and test tissues in solutions that allow precise control of hydration levels.

Declaration of competing interest

The authors declare that they have no known competing financial interests or personal relationships that could have appeared to influence the work reported in this paper.

Acknowledgements

The work was supported by the National Science Foundation (BMMB # 1760467).

Appendix A. Supplementary data

Supplementary data to this article can be found online at https://doi.org/10.1016/j.jmbbm.2021.104951.

References

Acaroglu, E.R., Iatridis, J.C., Setton, L.A., Foster, R.J., Mow, V.C., Weidenbaum, M., 1995 Dec 1. Degeneration and aging affect the tensile behavior of human lumbar anulus fibrosus. Spine 20 (24), 2690–2701.

Aladin, D.M., Cheung, K.M., Ngan, A.H., Chan, D., Leung, V.Y., Lim, C.T., Luk, K.D., Lu, W.W., 2010 Apr. Nanostructure of collagen fibrils in human nucleus pulposus and its correlation with macroscale tissue mechanics. J. Orthop. Res. 28 (4), 497–502.

Antoniou, J., Steffen, T., Nelson, F., Winterbottom, N., Hollander, A.P., Poole, R.A., Aebi, M., Alini, M., 1996 Aug 15. The human lumbar intervertebral disc: evidence for changes in the biosynthesis and denaturation of the extracellular matrix with growth, maturation, ageing, and degeneration. J. Clin. Invest. 98 (4), 996–1003.

Ateshian, G.A., Lai, W.M., Zhu, W.B., Mow, V.C., 1994 Nov 1. An asymptotic solution for the contact of two biphasic cartilage layers. J. Biomech. 27 (11), 1347–1360.

Ateshian, G.A., Chahine, N.O., Basalo, I.M., Hung, C.T., 2004 Mar 1. The correspondence between equilibrium biphasic and triphasic material properties in mixture models of articular cartilage. J. Biomech. 37 (3), 391–400.

Barthelemy, V.M., Van Rijsbergen, M.M., Wilson, W., Huyghe, J.M., Van Rietbergen, B., Ito, K., 2016 Feb 1. A computational spinal motion segment model incorporating a matrix composition-based model of the intervertebral disc. J. Mech. Behav. Biomed. Mater. 54, 194–204.

Beckstein, J.C., Sen, S., Schaer, T.P., Vresilovic, E.J., Elliott, D.M., 2008 Mar 15. Comparison of animal discs used in disc research to human lumbar disc: axial compression mechanics and glycosaminoglycan content. Spine 33 (6), E166–E173.

Bezci, S.E., Nandy, A., O'Connell, G.D., 2015 Oct 1. Effect of hydration on healthy intervertebral disk mechanical stiffness. J. Biomech. Eng. 137 (10).

Bezci, S.E., Werbner, B., Zhou, M., Malollari, K.G., Dorlhiac, G., Carraro, C., Streets, A., O'Connell, G.D., 2019 Sep. Radial variation in biochemical composition of the bovine caudal intervertebral disc. JOR spine 2 (3), e1065.

Bezci, S.E., Torres, K., Carraro, C., Chiavacci, D., Werbner, B., Lim, S., O'Connell, G.D., 2020 Dec 1. Transient swelling behavior of the bovine caudal disc. J. Mech. Behav. Biomed. Mater. 112, 104089.

Bloom, E.T., Lee, A.H., Elliott, D.M., 2021 Mar. Tendon multiscale structure, mechanics, and damage are affected by osmolarity of bath solution. Ann. Biomed. Eng. 49 (3), 1058–1068.

Buehler, M.J., Wong, S.Y., 2007 Jul 1. Entropic elasticity controls nanomechanics of single tropocollagen molecules. Biophys. J. 93 (1), 37–43.

Cao, L., Guilak, F., Setton, L.A., 2009 Sep. Pericellular matrix mechanics in the anulus fibrosus predicted by a three-dimensional finite element model and in situ morphology. Cell. Mol. Bioeng. 2 (3), 306–319.

Cassidy, J.J., Hiltner, A., Baer, E., 1989. Hierarchical structure of the intervertebral disc. Connect. Tissue Res. 23 (1), 75–88.

Castro, A.P., Alves, J.L., 2021 Jul 6. Numerical implementation of an osmo-poro-visco-hyperelastic finite element solver: application to the intervertebral disc. Comput. Methods Biomech. Biomed. Eng. 24 (5), 538–550.

Cortes, D.H., Jacobs, N.T., DeLucca, J.F., Elliott, D.M., 2014 Jun 27. Elastic, permeability and swelling properties of human intervertebral disc tissues: a benchmark for tissue engineering. J. Biomech. 47 (9), 2088–2094.

Costi, J.J., Hearn, T.C., Fazzalari, N.L., 2002 Jul 1. The effect of hydration on the stiffness of intervertebral discs in an ovine model. Clin. Biomech. 17 (6), 446–455.

Costi, J.J., Ledet, E.H., O'Connell, G.D., 2021 Mar. Spine biomechanical testing methodologies: the controversy of consensus vs scientific evidence. JOR spine 4 (1), e1138.

Davey, K.J., Skegg, D.C., 1971 Feb 1. The effects of high concentrations of an electrolyte on the swelling of non-metabolizing tissue slices. J. Physiol. 212 (3), 641–653.

Ebara, S., Iatridis, J.C., Setton, L.A., Foster, R.J., Mow, V.C., Weidenbaum, M., 1996 Feb 15. Tensile properties of nondegenerate human lumbar anulus fibrosus. Spine 21 (4), 452–461.

Ehlers, W., Karajan, N., Markert, B., 2009 Jun. An extended biphasic model for charged hydrated tissues with application to the intervertebral disc. Biomech. Model. Mechanobiol. 8 (3), 233–251.

Farndale, R.W., Sayers, C.A., Barrett, A.J., 1982 Jan 1. A direct spectrophotometric microassay for sulfated glycosaminoglycans in cartilage cultures. Connect. Tissue Res. 9 (4), 247–248.

Fratzl, P., Misof, K., Zizak, I., Rapp, G., Amenitsch, H., Bernstorff, S., 1998 Jan 1. Fibrillar structure and mechanical properties of collagen. J. Struct. Biol. 122 (1–2), 119–122.

Galante, J.O., 1967 May 1. Tensile properties of the human lumbar annulus fibrosus. Acta Orthop. Scand. 38 (Suppl. 100), 1–91.

Galbusera, F., Schmidt, H., Neidlinger-Wilke, C., Wilke, H.J., 2011a. The effect of degenerative morphological changes of the intervertebral disc on the lumbar spine biomechanics: a poroelastic finite element investigation. Comput. Methods Biomech. Biomed. Eng. 14 (8), 729–739.

Galbusera, F., Schmidt, H., Neidlinger-Wilke, C., Gottschalk, A., Wilke, H.J., 2011b. The mechanical response of the lumbar spine to different combinations of disc degenerative changes investigated using randomized poroelastic finite element models. Eur. Spine J. 20 (4), 563–571.

Gentleman, E., Lay, A.N., Dickerson, D.A., Nauman, E.A., Livesay, G.A., Dee, K.C., 2003 Sep 1. Mechanical characterization of collagen fibers and scaffolds for tissue engineering. Biomaterials 24 (21), 3805–3813.

Gregory, D.E., Callaghan, J.P., 2010 Sep 1. An examination of the influence of strain rate on subfailure mechanical properties of the annulus fibrosus. J. Biomech. Eng. (9), 132.

Gu, W.Y., Mao, X.G., Foster, R.J., Weidenbaum, M., Mow, V.C., Rawlins, B.A., 1999 Dec 1. The anisotropic hydraulic permeability of human lumbar anulus fibrosus: influence of age, degeneration, direction, and water content. Spine 24 (23), 2449.

Guo, Z., Shi, X., Peng, X., Caner, F., 2012 Jan 1. Fibre–matrix interaction in the human annulus fibrosus. J. Mech. Behav. Biomed. Mater. 5 (1), 193–205.

Han, W.M., Nerurkar, N.L., Smith, L.J., Jacobs, N.T., Mauck, R.L., Elliott, D.M., 2012 Jul. Multi-scale structural and tensile mechanical response of annulus fibrosus to osmotic loading. Ann. Biomed. Eng. 40 (7), 1610–1621.

Hollander, A.P., Heathfield, T.F., Webber, C., Iwata, Y., Bourne, R., Rorabeck, C., Poole, A.R., 1994 Apr 1. Increased damage to type II collagen in osteoarthritic articular cartilage detected by a new immunoassay. J. Clin. Invest. 93 (4), 1722–1732.

Holzapfel, G.A., Schulze-Bauer, C.A., Feigl, G., Regitnig, P., 2005 Mar. Single lamellar mechanics of the human lumbar anulus fibrosus. Biomech. Model. Mechanobiol. 3 (3), 125–140.
Huyghe, J.M., Jongeneelen, C.J., 2012 Jan. 3D non-affine finite strains measured in isolated bovine annulus fibrosus tissue samples. Biomech. Model. Mechanobiol. 11 (1), 161–170.
Iatridis, J.C., Setton, L.A., Foster, R.J., Rawlins, B.A., Weidenbaum, M., Mow, V.C., 1998 Jun 1. Degeneration affects the anisotropic and nonlinear behaviors of human anulus fibrosus in compression. J. Biomech. 31 (6), 535–544.
Isaacs, J.L., Vresilovic, E., Sarkar, S., Marcolongo, M., 2014 Dec 1. Role of biomolecules on annulus fibrosus micromechanics: effect of enzymatic digestion on elastic and failure properties. J. Mech. Behav. Biomed. Mater. 40, 75–84.
Jacobs, N.T., Cortes, D.H., Peloquin, J.M., Vresilovic, E.J., Elliott, D.M., 2014 Aug 22. Validation and application of an intervertebral disc finite element model utilizing independently constructed tissue-level constitutive formulations that are nonlinear, anisotropic, and time-dependent. J. Biomech. 47 (11), 2540–2546.
Katz, E.P., Li, S.T., 1973 Jan 19. The intermolecular space of reconstituted collagen fibrils. J. Mol. Biol. 73 (3), 351–369.
Lai WM, Hou JS, Mow VC. A Triphasic Theory for the Swelling and Deformation Behaviors of Articular Cartilage..
Lujan, T.J., Underwood, C.J., Jacobs, N.T., Weiss, J.A., 2009 Feb. Contribution of glycosaminoglycans to viscoelastic tensile behavior of human ligament. J. Appl. Physiol. 106 (2), 423–431.
Maas, S.A., Ellis, B.J., Ateshian, G.A., Weiss, J.A., 2012 Jan 1. FEBio: finite elements for biomechanics. J. Biomech. Eng. 134 (1).
Maroudas, A., Ziv, I., Weisman, N., Venn, M., 1985 Jan 1. Studies of hydration and swelling pressure in normal and osteoarthritic cartilage. Biorheology 22 (2), 159–169.
Monaco, L.A., DeWitte-Orr, S.J., Gregory, D.E., 2016 Feb. A comparison between porcine, ovine, and bovine intervertebral disc anatomy and single lamella annulus fibrosus tensile properties. J. Morphol. 277 (2), 244–251.
Mow, V.C., Kuei, S.C., Lai, W.M., Armstrong, C.G., 1980 Feb 1. Biphasic creep and stress relaxation of articular cartilage in compression: theory and experiments. J. Biomech. Eng. 102 (1), 73–84.
Mow, V.C., Holmes, M.H., Lai, W.M., 1984 Jan 1. Fluid transport and mechanical properties of articular cartilage: a review. J. Biomech. 17 (5), 377–394.
Natarajan, R.N., Williams, J.R., Andersson, G.B., 2006 Apr 1. Modeling changes in intervertebral disc mechanics with degeneration. JBJS 88 (Suppl. l_2), 36–40.
O'Connell, G.D., Leach, J.K., Klineberg, E.O., 2015 Nov 1. Tissue engineering a biological repair strategy for lumbar disc herniation. BioResearch Open Access 4 (1), 431–445.
Partanen, J.I., Partanen, L.J., Vahteristo, K.P., 2017 Sep 14. Traceable thermodynamic quantities for dilute aqueous sodium chloride solutions at temperatures from (0 to 80) C. Part 1. Activity coefficient, osmotic coefficient, and the quantities associated with the partial molar enthalpy. J. Chem. Eng. Data 62 (9), 2617–2632.
Paul Buckley, C., Samuel Salisbury, S.T., Zavatsky, A.B., 2016 Oct 1. Viscoelasticity of tendons under transverse compression. J. Biomech. Eng. 138 (10).
Perie, D.S., Maclean, J.J., Owen, J.P., Iatridis, J.C., 2006 May. Correlating material properties with tissue composition in enzymatically digested bovine annulus fibrosus and nucleus pulposus tissue. Ann. Biomed. Eng. 34 (5), 769–777.
Pezowicz, C.A., Robertson, P.A., Broom, N.D., 2005 Oct. Intralamellar relationships within the collagenous architecture of the annulus fibrosus imaged in its fully hydrated state. J. Anat. 207 (4), 299–312.
Pflaster, D.S., Krag, M.H., Johnson, C.C., Haugh, L.D., Pope, M.H., 1997 Jan 15. Effect of test environment on intervertebral disc hydration. Spine 22 (2), 133–139.
Pham, D.T., Shapter, J.G., Costi, J.J., 2018 Jan 23. Tensile behaviour of individual fibre bundles in the human lumbar anulus fibrosus. J. Biomech. 67, 24–31.
Rijsbergen, M.V., van Rietbergen, B., Barthelemy, V., Eltes, P., Á, Lazáry, Lacroix, D., Noailly, J., Ho, Ba, Tho, M.C., Wilson, W., Ito, K., 2018 Aug 30. Comparison of patient-specific computational models vs. clinical follow-up, for adjacent segment disc degeneration and bone remodeling after spinal fusion. PLoS One 13 (8), e0200899.
Robinson, J.R., 1978 Sep 1. Control of water content of respiring kidney slices by sodium chloride and polyethylene glycol. J. Physiol. 282 (1), 285–294.
Roeder, B.A., Kokini, K., Sturgis, J.E., Robinson, J.P., Voytik-Harbin, S.L., 2002 Apr 1. Tensile mechanical properties of three-dimensional type I collagen extracellular matrices with varied microstructure. J. Biomech. Eng. 124 (2), 214–222.
Safa, B.N., Meadows, K.D., Szczesny, S.E., Elliott, D.M., 2017 Aug 16. Exposure to buffer solution alters tendon hydration and mechanics. J. Biomech. 61, 18–25.
Safa, B.N., Bloom, E.T., Lee, A.H., Santare, M.H., Elliott, D.M., 2020 Aug 26. Evaluation of transverse poroelastic mechanics of tendon using osmotic loading and biphasic mixture finite element modeling. J. Biomech. 109, 109892.
Schiller, L.R., Emmett, M., Santa Ana, C.A., Fordtran, J.S., 1988 Apr 1. Osmotic effects of polyethylene glycol. Gastroenterology 94 (4), 933–941.
Schmidt, H., Shirazi-Adl, A., Schilling, C., Dreischarf, M., 2016 Jun 14. Preload substantially influences the intervertebral disc stiffness in loading–unloading cycles of compression. J. Biomech. 49 (9), 1926–1932.
Screen, H.R., Shelton, J.C., Chhaya, V.H., Kayser, M.V., Bader, D.L., Lee, D.A., 2005 Aug. The influence of noncollagenous matrix components on the micromechanical environment of tendon fascicles. Ann. Biomed. Eng. 33 (8), 1090–1099.
Screen, H.R., Chhaya, V.H., Greenwald, S.E., Bader, D.L., Lee, D.A., Shelton, J.C., 2006 Sep 1. The influence of swelling and matrix degradation on the microstructural integrity of tendon. Acta Biomater. 2 (5), 505–513.
Shen, Z.L., Dodge, M.R., Kahn, H., Ballarini, R., Eppell, S.J., 2008 Oct 15. Stress-strain experiments on individual collagen fibrils. Biophys. J. 95 (8), 3956–3963.
Showalter, B.L., Beckstein, J.C., Martin, J.T., Beattie, E.E., Orías, A.A., Schaer, T.P., Vresilovic, E.J., Elliott, D.M., 2012 Jul 1. Comparison of animal discs used in disc research to human lumbar disc: torsion mechanics and collagen content. Spine 37 (15), E900.
Skaggs, D.L., Weidenbaum, M., Iatridis, J.C., Ratcliffe, A., Mow, V.C., 1994 Jun 1. Regional variation in tensile properties and biochemical composition of the human lumbar anulus fibrosus. Spine 19 (12), 1310–1319.
Spencer AJ. Deformations of Fibre-Reinforced Materials..
Stegemann, H., Stalder, K., 1967 Nov 1. Determination of hydroxyproline. Clin. Chim. Acta 18 (2), 267–273.
Sverdlik, A., Lanir, Y., 2002 Feb 1. Time-dependent mechanical behavior of sheep digital tendons, including the effects of preconditioning. J. Biomech. Eng. 124 (1), 78–84.
Thorpe, C.T., Screen, H.R., 2016. Tendon structure and composition. Metabolic Influences on Risk for Tendon Disorders 3–10.
Urban, J.P., Maroudas, A., 1979 Aug 6. The measurement of fixed charged density in the intervertebral disc. Biochim. Biophys. Acta Gen. Subj. 586 (1), 166–178.
Urban, J.P., Maroudas, A., 1981 Jan 1. Swelling of the intervertebral disc in vitro. Connect. Tissue Res. 9 (1), 1, 0.
Van Der Rijt, J.A., Van Der Werf, K.O., Bennink, M.L., Dijkstra, P.J., Feijen, J., 2006 Sep 15. Micromechanical testing of individual collagen fibrils. Macromol. Biosci. 6 (9), 697–702.
Werbner B, Lee M, Lee A, Yang L, Habib M, Fields AJ, O'Connell GD. Non-enzymatic glycation of annulus fibrosus alters tissue-level failure mechanics in tension. J. Mech. Behav. Biomed. Mater.. In-review..
Werbner, B., Zhou, M., O'Connell, G.D., 2017 Nov 1. A novel method for repeatable failure testing of annulus fibrosus. J. Biomech. Eng. 139 (11).
Werbner, B., Spack, K., O'Connell, G.D., 2019 May 24. Bovine annulus fibrosus hydration affects rate-dependent failure mechanics in tension. J. Biomech. 89, 34–39.
Wilson, W., Huyghe, J.M., Van Donkelaar, C.C., 2007 Jan. Depth-dependent compressive equilibrium properties of articular cartilage explained by its composition. Biomech. Model. Mechanobiol. 6 (1), 43–53.
Yang, B., O'Connell, G.D., 2019 Dec 1. Intervertebral disc swelling maintains strain homeostasis throughout the annulus fibrosus: a finite element analysis of healthy and degenerated discs. Acta Biomater. 100, 61–74.
Yang, B., O'Connell, G.D., 2018 Jun 1. Swelling of fiber-reinforced soft tissues is affected by fiber orientation, fiber stiffness, and lamella structure. J. Mech. Behav. Biomed. Mater. 82, 320–328.
Żak, M., Pezowicz, C., 2016 Sep. Analysis of the impact of the course of hydration on the mechanical properties of the annulus fibrosus of the intervertebral disc. Eur. Spine J. 25 (9), 2681–2690.
Zhou, M., Bezci, S.E., O'Connell, G.D., 2019 Nov 4. Multiscale composite model of fiber-reinforced tissues with direct representation of sub-tissue properties. Biomech. Model. Mechanobiol. 1–5.
Zhou, M., Lim, S., O'Connell, G.D., 2021a. A robust multiscale and multiphasic structure-based modeling framework for the intervertebral disc. Front. Bioeng. Biotechnol. 9, 685799.
Zhou, M., Werbner, B., O'Connell, G.D., 2021b. Fiber engagement accounts for geometry-dependent annulus fibrosus mechanics: a multiscale, Structure-Based Finite Element Study. J. Mech. Behav. Biomed. Mater. 115, 104292.